DOI: 10.21062/mft.2026.046 © 2026 Manufacturing Technology. All rights reserved. http://www.journalmt.com

Effect of Liquid Nitrogen Cooling on Machinability and Tool Wear Mechanisms in Cutting CGI-400

Shanshan Xu (0009-0002-6645-5035)[1], Xu Sun (0009-0007-3706-172X)[2], Fanning Meng (0009-0007-4639-7372)[1], Yingqi Shen (0009-0006-4455-2669)[1], Chunjing Shi (0009-0002-4853-432X)[1], Ying Yang (0000-0002-1030-779X)[1]
[1]School of Mechanical Engineering, Hangzhou Dianzi University, Hangzhou 310018, China.
*E-mail: mfn@hdu.edu.cn
[2]Hangzhou Shuzhi Innovation Transportation Technology Development Co., Ltd., Hangzhou 310000, China

This study systematically investigates the performance of liquid nitrogen cooling in machining compacted graphite iron 400 (CGI-400), compared with conventional cutting fluid cooling, focusing on mechanical properties, cutting temperature, tool wear, and surface quality. Results indicate that liquid nitrogen cooling significantly reduces the cutting temperature by 22.38%, effectively suppresses flank wear and built-up edge formation, and demonstrates remarkable advantages at cutting lengths beyond 3000 m. Cryogenic embrittlement of CGI-400 under liquid nitrogen leads to an 11.32% reduction in tensile strength, while the temperature-dependent thermal conductivity influences heat management in the cutting zone. EDS analysis reveals less material adhesion and improved coating integrity under liquid nitrogen cooling, contributing to prolonged tool life and enhanced surface finish. This research provides theoretical and practical insights into the cryogenic machining of CGI-400.

Keywords: Liquid nitrogen cooling, CGI-400, Tool wear, Cutting temperature, Surface roughness

1 Introduction

With the global automotive industry rapidly developing towards high efficiency, energy saving, lightweight, and high reliability, core components such as engines and braking systems have imposed strict requirements on the comprehensive performance of materials [1]. CGI, featuring a unique coral-like three-dimensional graphite structure, integrates the high strength and wear resistance of nodular cast iron with the excellent castability, thermal conductivity, and damping properties of gray cast iron (GCI) [2-3]. This performance advantage makes CGI an ideal material to meet the harsh working conditions of engine turbocharging and downsizing, and it has been widely used in the manufacturing of key components such as diesel engine blocks [4], cylinder heads [5], and brake discs [6]—industrial statistics show that the global output of CGI engines exceeded 8 million units in 2024 [7]. Its machining quality directly determines the operational efficiency and service life of power systems [8], and the breakthrough of large-scale machining technology is of great engineering significance for promoting the upgrading of the automotive industry.

However, the machining process of CGI faces multiple technical bottlenecks and is recognized as a typical difficult-to-machine materiál [9]. Firstly, the thermal conductivity of CGI is only about 37 W/(mK), approximately 77% of that of GCI, so heat in the cutting zone is easy to accumulate, which accelerates thermal softening and diffusion wear of the tool [10-11]. Secondly, the tensile strength of CGI-400 reaches 400 MPa, much higher than that of GCI (250 MPa), resulting in significantly increased cutting forces and a flank wear rate 50%~80% higher than that of GCI[12-14]. Thirdly, the sulfur content in CGI is extremely low, failing to form lubricating protective films like MnS in GCI, and the friction coefficient between the tool and chips increases to 0.6~0.8 [15]. In addition, the microstructural evolution of CGI during high-temperature cutting further exacerbates machining difficulties; Venugopal Rao et al. found that the wear behavior of CGI at 200 °C is significantly different from that at room temperature, indicating the importance of cooling control for CGI machining [16]. These problems result in low machining efficiency and high costs, severely restricting its large-scale application.

In terms of cooling and lubrication technology optimization [17], conventional methods have problems such as environmental pollution and high waste liquid treatment costs, gradually failing to meet the needs of green manufacturing [18], and cryogenic cooling technology has become a core research direction in CGI machining. Suhaimi et al. [19] designed an indirect liquid nitrogen spray system, delivering liquid nitrogen to the cutting zone through customized conical nozzles to avoid microcracks

caused by direct impact of liquid nitrogen on the workpiece. In high-speed CGI milling, the tool life was increased by 26%, and the cutting temperature was reduced by 18%~22%; Meng et al. [20] proposed a composite scheme of "liquid nitrogen cooling the rake face+MQL lubricating the flank face" based on boundary layer theory, using the negative gradient pressure formed by the relative movement of tool and workpiece to promote uniform distribution of MQL oil film on the secondary flank face. This not only reduced the cutting force by 17.7% and extended the tool life by 34.6%; Tu et al. [21] developed supercritical CO_2-based MQL technology, using the high permeability of supercritical CO_2 to deliver plant-based lubricating media to the tool-chip interface. In CGI milling, the cutting temperature was reduced by 30%~40%, the surface roughness by 15%~42%, and the cutting fluid consumption was reduced by more than 90%.

In addition, research on the adaptability of single cryogenic cooling has also made progress: Lin et al. [22] explored the effect of pure liquid nitrogen jetting on CGI turning, and found that liquid nitrogen can control the tool edge temperature below 600 °C through rapid phase change heat absorption, significantly inhibiting the diffusion wear of WC-Co tools, but microcracks are prone to occur on the surface due to excessive temperature difference of the workpiece when used alone; Kuzu et al. [23] compared three cooling mediaand found that liquid nitrogen has more significant advantages at high cutting speeds (tool life increased by 20%~25%), while MQL has better lubrication effects at medium and low speeds; Tooptong et al. [24] also found that TiCN-coated tools have the best compatibility with liquid nitrogen cooling, and the thermal stability of the coating is improved in a low-temperature environment, reducing the wear rate by 40% compared to uncoated tools.

In summary, existing studies have demonstrated the potential of cryogenic cooling technology in improving the machinability of CGI, particularly in reducing cutting temperature and suppressing tool wear. However, systematic investigations into the influence of liquid nitrogen cooling on the mechanical properties of CGI and its mechanism in maintaining coating integrity and surface quality during prolonged machining remain limited.

Aiming at the problems of high cutting temperature, severe tool wear, and insufficient optimization of cooling technology in CGI machining, this paper systematically studies the influence laws of cutting fluid cooling and liquid nitrogen cooling on CGI cutting temperature, surface roughness, and flank wear, and reveals the mechanism of cryogenic cooling. Through experiments, the machining performance under different cooling methods is compared, providing theoretical support and technical reference for the efficient and high-precision machining of CGI.

2 Experimental procedures

2.1 Experimental materials

The material used in this work was CGI-400, procured from Weichai Power Co., Ltd. (Weifang, China). As illustrated in Fig. 1(a), the as-received material was a hollow cylinder with an outer diameter (D_1) of 200 mm, an inner diameter (D_2) of 120 mm, and a height (H) of 150 mm. For metallographic examination, a small sample was excised, which subsequently underwent grinding, polishing, and etching with picric acid to reveal the characteristic microstructure of CGI-400, presented in Fig. 1(b). The metallographic image reveals that the CGI-400 microstructure consists of worm-shaped graphite surrounded by ferrite, all within a predominantly pearlitic matrix [25].

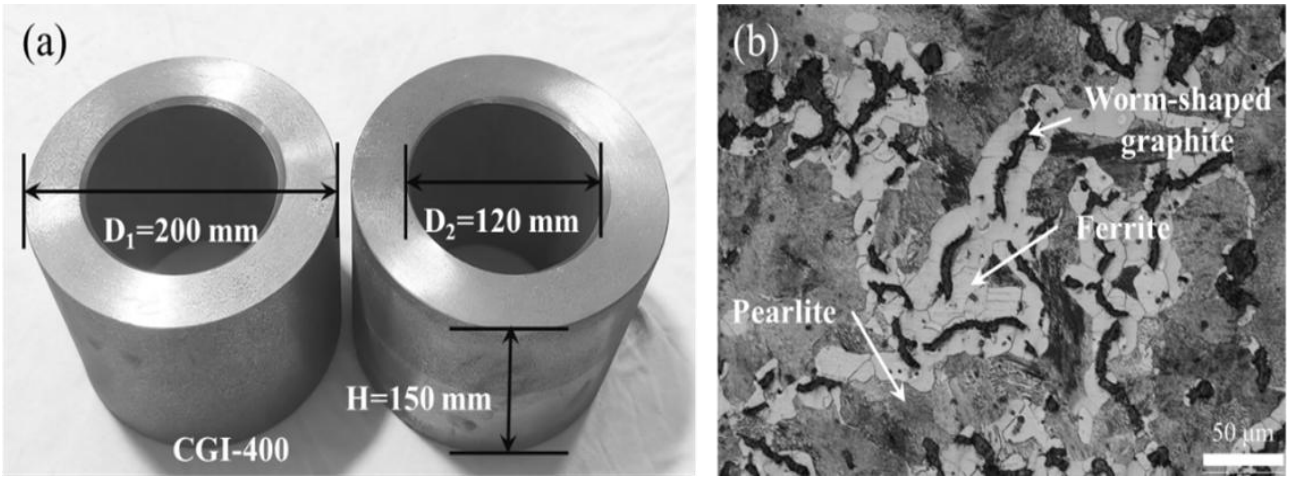


Fig. 1 *CGI-400 Material: (a) Physical Specimen and (b) Metallographic Image*

2.2 Performance testing of CGI-400

To investigate the variation in mechanical properties of CGI-400 under cryogenic conditions, tensile specimens were immersed in liquid nitrogen for 15 minutes to allow the temperature to equilibrate. The specimens were then rapidly removed and subjected to tensile testing. The specimen geometry conformed to the Chinese National Standard GB/T 228.1-2010 (Metallic Materials-Tensile Testing-Part 1: Method of Test at Room Temperature), as illustrated in Fig. 2(a). Fig. 2(b-c) show the physical specimens before and after tensile fracture, respectively. The tests were performed using an electronic universal testing machine (DNS100, Changchun Institute of Mechanical Science Co., Ltd., China). The ultimate tensile strength results for CGI-400 under both liquid nitrogen-cooled and room temperature conditions are presented in Tab. 1. The reported values represent the average of three tests, with the standard deviation calculated accordingly.

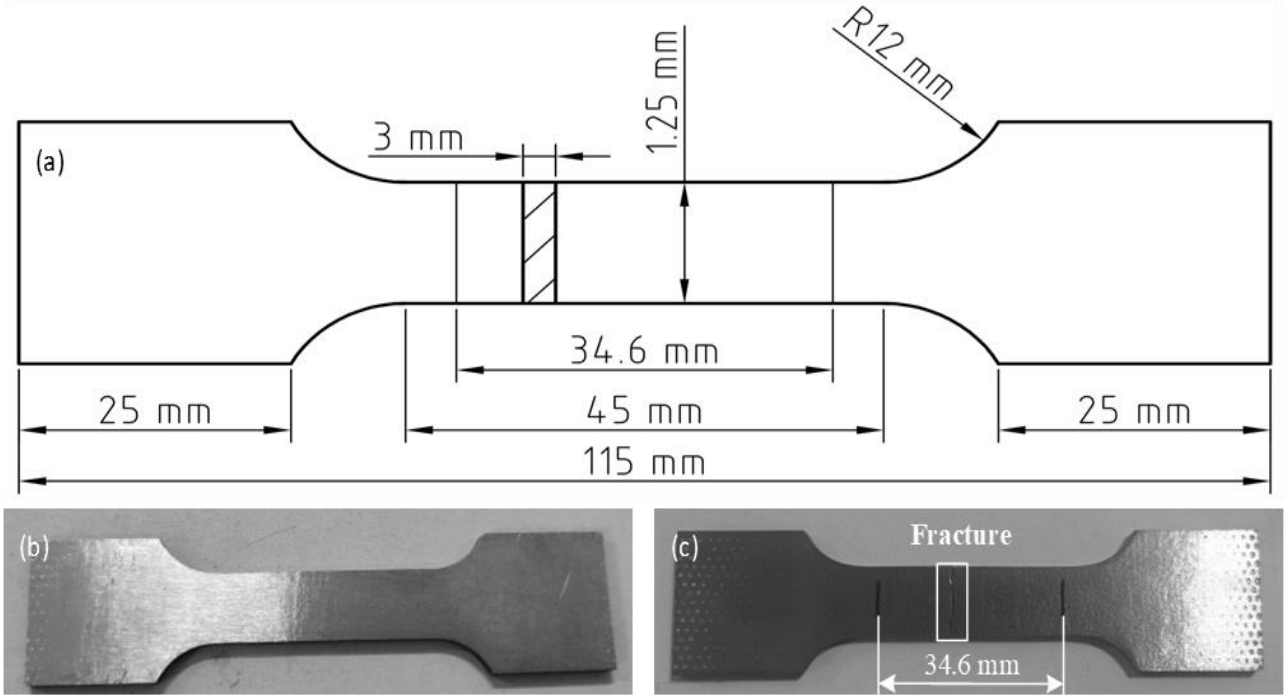


Fig. 2 *(a) Tensile Specimen Geometry, (b) Physical Specimen Before Testing, and (c) Physical Specimen After Fracture*

Tab. 1 *Tensile Properties of CGI-400 under Different Temperatures*

Temperatures	No.	Maximum load/ KN	Cross sectional area/ mm²	Tensile strength/ MPa	Average tensile strength (Rm)/ MPa	Standard Deviation (S)
Liquid nitrogen immersion	1	11.98	37.5	319.5	331.5	9.88
	2	12.42		331.2		
	3	12.89		343.7		
Room temperature	1	13.90	37.5	370.7	373.8	4.96
	2	13.87		369.9		
	3	14.28		380.8		

Thermal conductivity is a crucial parameter affecting the machinability of materials, especially at elevated temperatures. This study investigated the thermal conductivity of CGI-400 across different temperatures (room temperature, 100°C, 200°C, and 300°C). The measurements were conducted using a thermal constants analyzer (Hot Disk TPS 2500S, Sweden) on specimens machined into cylindrical shapes with a diameter of 75 mm and height of 22 mm. The test conditions and corresponding results are presented in Tab. 2.

Tab. 2 *Test Results of Thermal Conductivity*

Test temperature	Test conditions			Thermal conductivity / W/mK			Average	Standard deviation
	Power/ Mw	Heating time/ s	Temperature / ℃	1	2	3		
Room temperature	800	2.5	23	33.96	33.89	33.98	33.94	0.04
100	1000	10	100	32.64	31.55	31.79	31.99	0.47
200	1100	10	200	29.93	30.41	31.33	30.56	0.58
300	1100	10	300	29.99	29.76	29.75	29.83	0.11

2.3 Machining tests

Based on previous experimental work, the Walter CCGT060208-MK4 WKK20S cutting insert was selected for this investigation. The insert geometry is shown in Fig. 3(a), with a physical photograph presented in Fig. 3(b). The physical details of the insert are provided in Tab. 3. To measure the cutting temperature during CGI-400 machining, a 1 mm diameter hole was fabricated using electrical discharge machining at a location 1 mm from the tool tip.

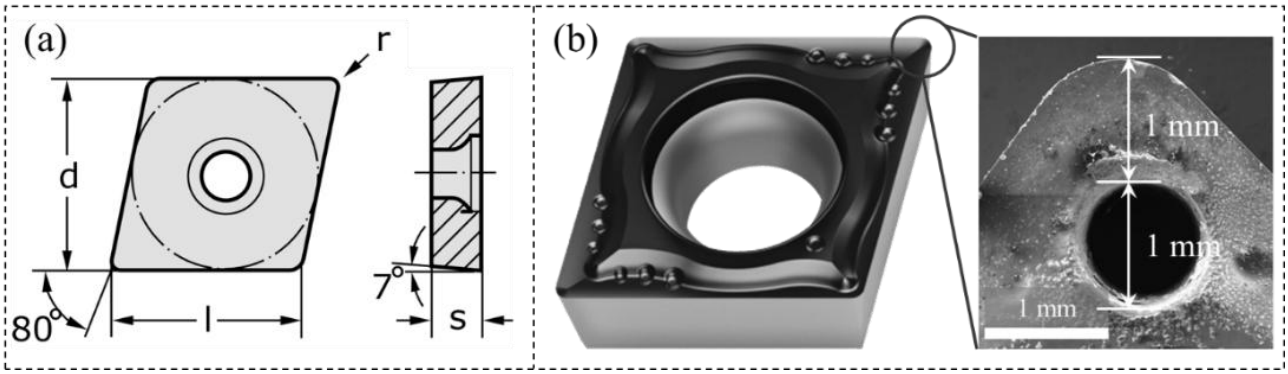


Fig. 3 *Cutting insert: (a) schematic diagram of the geometry, (b) physical photograph*

Tab. 3 *The physical details of CCGT060208-MK4 WKK20S*

Diameter of inscribed circle (d)	Insert thickness (s)	Radius (r)	Cutting edge length (l)	Clearance angle major (α)
6.35 mm	2.38 mm	0.8 mm	6.45 mm	7°

To measure the cutting temperature when machining CGI-400, this paper designs a wireless monitoring system for cutting temperature during turning operations. The measurement system is illustrated in Fig. 4. As shown in Fig. 4, the system consists of two main components: the machining system and the monitoring system. The machining system primarily includes the insert, tool holder, and tool post. The monitoring system mainly comprises a thermocouple sensor, an intelligent wireless temperature and humidity acquisition device, and a computer. The tip of the thermocouple sensor is placed into a pre-drilled hole in the insert and sealed with silicone to prevent contact with cutting fluid or liquid nitrogen, which could affect measurement accuracy.

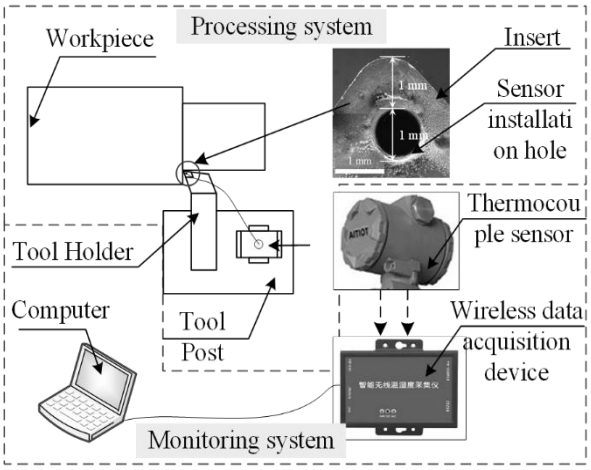


Fig. 4 *Schematic Diagram of the Wireless Cutting Temperature Measurement System Structure*

The liquid nitrogen cooling cutting tests were conducted on an HTC3650 CNC lathe (Shenyang Machine Tool). Liquid nitrogen was stored in a self-pressurized Dewar tank and delivered directly to the tool-workpiece interface (rake face) through freeze-resistant tubing. The injection pressure of liquid nitrogen is set to 0.3 MPa. The cutting parameters were optimized values obtained from previous orthogonal experiments, specifically set at v=200 m/min, f=0.1 mm/rev, and a_p=0.1 mm [20, 26-27].

Surface roughness measurements were performed using a portable roughness tester (TR2000, Beijing Times, China). Tool wear was examined with a CCD high-definition microscope (GP-300C, Kunshan Gaoce Precision Instrument, China). Additionally, flank wear was investigated using a scanning electron microscope (SEM, Quanta 200F, FEI, USA) integrated with an energy dispersive X-ray spectroscopy (EDS) system.

3 Results and discussion

3.1 Physical properties of CGI-400 under different temperatures

Fig. 5(a) presents a comparison of the tensile strength of CGI-400 between room temperature and after cryogenic treatment with liquid nitrogen. It was observed that the treatment reduced the tensile strength from 373.8 MPa to 331.5 MPa, a decrease of approximately 11.32%. The decrease in the tensile strength of CGI-400 after immersion in liquid nitrogen is attributed to changes in its internal microscopic phases caused by the extremely low temperature. Examination of the metallograph of CGI-400 (Fig. 1(b)) reveals a microstructure comprising primarily worm-shaped graphite, ferrite, and pearlite, wherein the graphite is enveloped by ferrite, and the ferrite is embedded in the pearlite matrix. The literature indicates that the thermal expansion coefficient (CTE) of graphite is in the range of 2-5×10^{-6} /K, which is considerably lower than that of the ferritic-pearlitic iron matrix (approximately 9-12×10^{-6} /K) [28]. Consequently, when CGI-400 is immersed in liquid nitrogen, the differing CTEs result in unequal contraction among these phases. This generates micro-cracks in the microstructure, thereby degrading the tensile strength of the material.

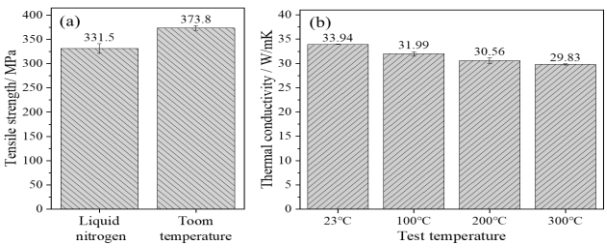


Fig. 5 *Physical Properties of CGI-400 Under Different Temperatures: (a) Tensile Strength, (b) Thermal Conductivity*

As shown in Fig. 5(b), for the CGI-400 material, its thermal conductivity exhibits a continuous and relatively uniform decreasing trend as the test temperature increases. At 23°C (room temperature), the thermal conductivity reaches 33.94 W/mK, demonstrating good thermal conductivity at room temperature. When the temperature rises to 100°C, the thermal conductivity decreases to 31.99 W/mK, with a reduction of approximately 5.7%. When further increasing to 200°C, the thermal conductivity is 30.56 W/mK, a decrease of about 10.0% compared to room temperature. When the temperature reaches 300°C, the thermal conductivity drops to 29.83 W/mK, with a decrease of about 12.1% relative to room temperature. This variation indicates that temperature is a key factor affecting the thermal conductivity of CGI-400 material. As the temperature increases, the heat conduction mechanisms inside the material change, leading to a gradual weakening of thermal conductivity.

3.2 Cutting surface roughness under different cooling methods

The variations of surface roughness (Ra) and flank face wear with cutting length under liquid nitrogen cooling and cutting fluid cooling are presented in Tab. 4 and Fig. 6. As observed, with the increase of cutting length, both surface roughness and flank face wear exhibit a continuous increasing trend under both cooling methods. This phenomenon is attributed to the cumulative tool wear and the intensified mechanical interaction between the tool and workpiece during prolonged cutting.

For the surface roughness of CGI-400 after cutting, as depicted in Fig. 6(a), when the cutting length is less than 3000 m, the surface roughness values under liquid nitrogen cooling and cutting fluid cooling are basically consistent, indicating that both cooling methods have comparable effects on controlling surface finish in this stage. However, when the cutting length exceeds 3000 m, a significant difference in surface roughness emerges. Specifically, the surface roughness under cutting fluid cooling increases sharply and then stabilizes at approximately 2.3–2.4 μm. In contrast, the surface roughness under liquid nitrogen cooling remains stable at around 2.1–2.2 μm, demonstrating better stability and lower surface roughness during prolonged machining.

As observed in Fig. 6(b), the progression of flank wear follows a trend similar to that of surface roughness. When the cutting length is less than 3000 m, the flank wear values under both cooling conditions remain comparable. However, beyond the 3000 m mark, a significant divergence emerges: the flank wear under cutting fluid cooling begins to widen considerably compared to that under liquid nitrogen cooling. This indicates that employing liquid nitrogen

cooling for machining CGI-400 effectively suppresses flank wear, thereby extending tool life.

Regarding the flank face wear, a similar staged variation is observed. When the cutting length is less than 3000 m, the flank face wear under both cooling methods increases at a comparable rate and reaches similar values. Once the cutting length exceeds 3000 m, the flank face wear under cutting fluid cooling rises sharply, while that under liquid nitrogen cooling increases relatively gently and remains at a significantly lower level. For instance, after 3000 m, the flank face wear under cutting fluid cooling escalates rapidly, whereas liquid nitrogen cooling restrains the wear growth, showcasing its superior ability to prolong tool life in prolonged machining.

The aforementioned analysis reveals an interesting phenomenon: a distinct transition at a cutting length of 3000 m is observed for both the surface roughness of the machined workpiece and the flank wear of the tool when machining CGI-400 under the two cooling conditions. Below this 3000 m threshold, both the surface roughness and flank wear values remain nearly identical under both cooling methods. The significant divergence between them primarily occurs after the cutting length exceeds 3000 m. This phenomenon can be attributed to the following combined reasons:

Firstly, when the cutting length is less than 3000 m, the heat accumulation in the tool and workpiece is relatively low; however, it increases progressively with further cutting. Secondly, a coated cutting tool was used in this study. During the initial stage (below 3000 m), the tool coating is not fully worn. The flank wear involves friction between the workpiece and the hard, wear-resistant coating material, which also exhibits low adhesion to the chip. Consequently, wear is minimal. When the cutting length exceeds 3000 m, the tool coating is completely worn away under cutting fluid cooling. In contrast, the tool flank under liquid nitrogen cooling maintains a relatively intact coating due to the ultra-low temperature effect of liquid nitrogen. This fundamental difference in coating integrity leads to the markedly different performance observed.

Tab. 4 *Data of Surface Roughness and Flank Face Wear for Machining CGI-400*

Cutting length/ m	Liquid nitrogen cooling				Cutting fluid cooling			
	Surface roughness (Ra) / μm		Flank face wear / μm		Surface roughness (Ra) / μm		Flank face wear / μm	
	Average	Standard deviation	Average	Standard deviation	Average	Standard deviation	Average	Standard deviation
500	1.252	0.02	38.3	3.41	1.277	0.031	40.8	4.13
1000	1.33	0.024	62.1	4.23	1.344	0.024	63.6	5.70
1500	1.673	0.031	70.4	5.12	1.64	0.015	72.9	3.24
2000	1.829	0.015	84.2	4.46	1.789	0.022	88.9	4.62
2500	1.884	0.041	90.7	2.71	1.891	0.046	95.8	6.74
3000	2.051	0.032	106.1	6.83	2.023	0.039	110.5	4.28
3500	2.119	0.05	110.3	4.92	2.371	0.054	125.2	7.32
4000	2.125	0.052	120.5	7.14	2.372	0.048	140.4	6.23
4500	2.166	0.063	129.9	5.43	2.415	0.055	162.1	5.50
5000	2.195	0.044	134.7	4.61	2.429	0.043	174.6	8.13

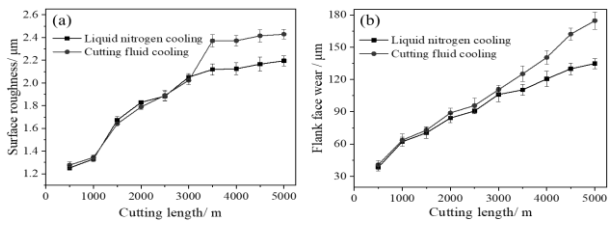


Fig. 6 *Variations of Surface Roughness (a) and Flank Face Wear (b) Under Liquid Nitrogen Cooling and Cutting Fluid Cooling*

3.3 Mechanism of flank face wear

Optical images of the tool flank face wear at different cutting lengths (1000 m, 3000 m,5000 m) are presented in Fig. 7. A clear comparison in Fig. 8 reveals that material adhesion and built-up edge formation on the flank face are significantly more pronounced under cutting fluid cooling compared to liquid nitrogen cooling.

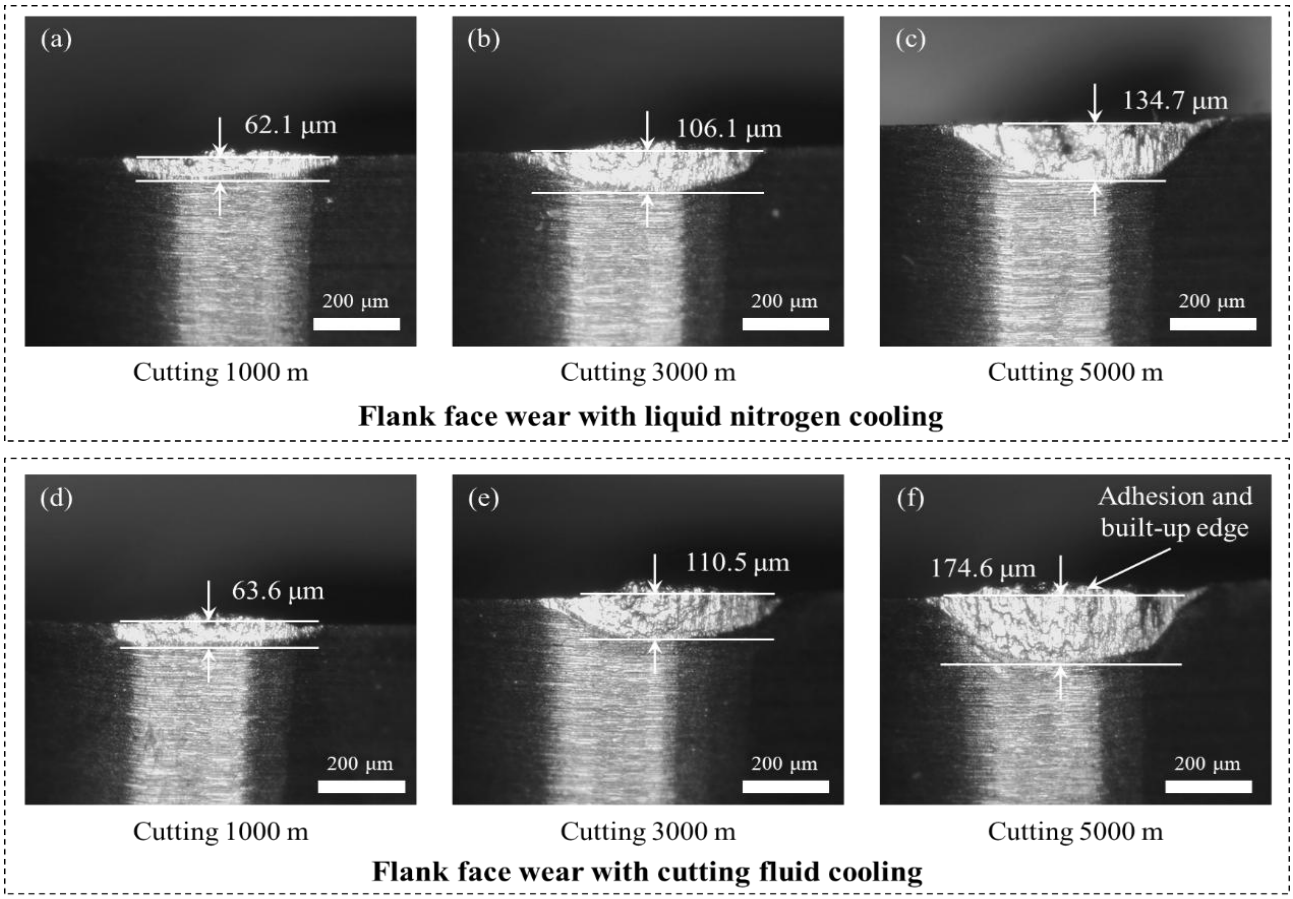


Fig. 7 *Optical Images of the Flank Face Wear for Cutting CGI-400: (a-c) Liquid Nitrogen Cooling, and (d-f) Cutting Fluid Cooling*

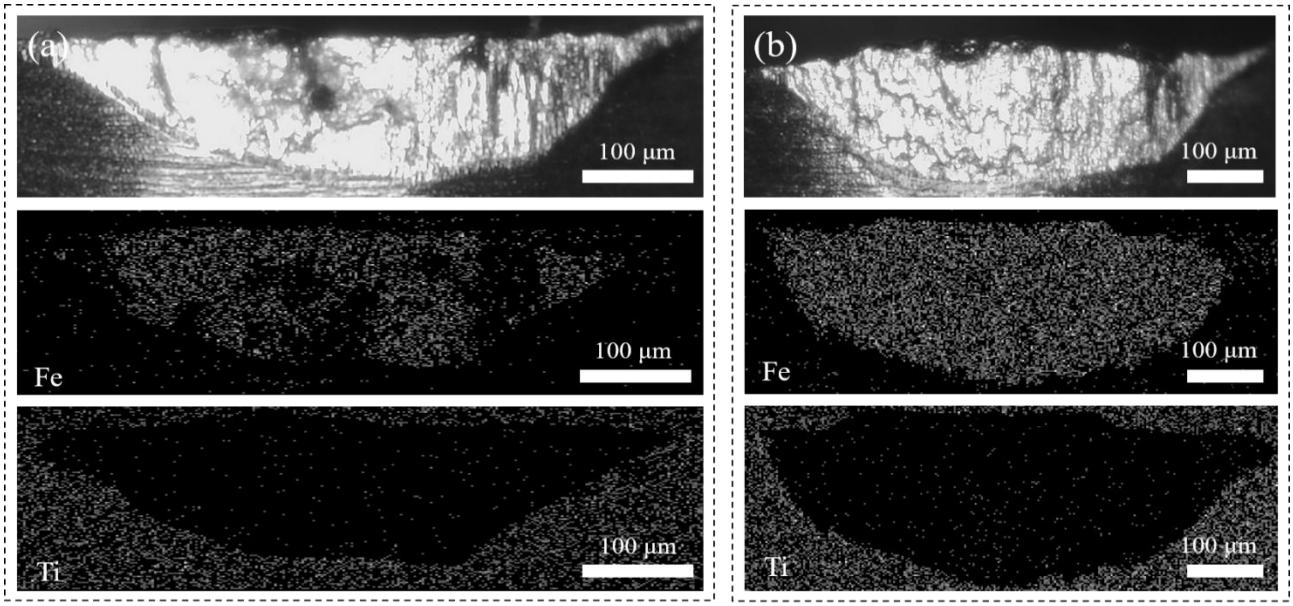


Fig. 8 *EDS Results of the Flank Face Wear: (a) Liquid Nitrogen Cooling, (b) Cutting Fluid Cooling*

Fig. 8 shows the surface morphology of flank wear and EDS test results after cutting 5000m using liquid nitrogen cooling and cutting fluid cooling. This examination primarily focuses on the main workpiece material Fe and the primary coating material Ti of the tool. It is clearly evident that the tool wear area is predominantly composed of Fe elements, indicating substantial chip adhesion on the flank face. The adhered chips protrude above the rake face, consequently forming a built-up edge. The areas beyond the wear zone retain intact coating. Moreover, by comparing the distribution of Fe elements in

the wear areas under both cooling conditions, it can be observed that when using liquid nitrogen cooling, there is less material adhesion with some areas remaining uncovered, and no built-up edge is formed. In contrast, during machining with cutting fluid, the entire wear area is covered by chips.

3.4 Cutting temperature

The cutting temperature test results clearly demonstrate that liquid nitrogen cooling exhibits remarkable advantages in controlling cutting temperature. In Fig. 9(a), the real-time temperature curve shows that the cutting temperature under cutting fluid cooling (red curve) is consistently higher than that under liquid nitrogen cooling (black curve), with relatively obvious fluctuations. The average temperature data in Fig. 9(b) further quantifies this difference, where the average cutting temperature of cutting fluid cooling is 260.1°C, while with liquid nitrogen cooling, it is reduced to 201.9°C, representing a 22.38% decrease. This result is attributed to the strong cryogenic cooling characteristic of liquid nitrogen, which can quickly take away the heat in the cutting zone and effectively suppress the increase of cutting temperature.

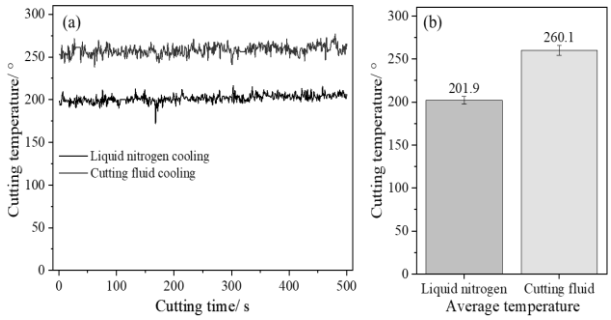


Fig. 9 *The Cutting Temperature of Tool Tip: (a) Real-time Cutting Temperature Under Steady State, (b) Average Cutting Temperature*

3.5 Discussion

The experimental results reveal a sophisticated interplay between the cryogenic properties of CGI-400 and its machining performance under liquid nitrogen cooling. The interconnected effects of material behavior, thermal management, and tool wear create a self-reinforcing cycle that fundamentally distinguishes cryogenic machining from conventional cooling methods.

3.5.1 Material-tool interaction mechanism

The 11.32% reduction in tensile strength after liquid nitrogen immersion demonstrates significant cryogenic embrittlement in CGI-400. This property alteration directly affects chip formation and tool-workpiece interaction. The brittle material behavior under cryogenic conditions promotes discontinuous chip formation, reducing the contact area and adhesion tendency between the tool and workpiece. This mechanism is clearly evidenced by the EDS analysis, which shows substantially less Fe element transfer to the tool flank face under liquid nitrogen cooling compared to cutting fluid condition.

Simultaneously, the temperature-dependent thermal conductivity of CGI-400 creates a critical thermal management challenge. As the thermal conductivity decreases by 12.1% at 300°C, heat accumulation accelerates during machining. Under conventional cooling, this establishes a vicious cycle: reduced heat dissipation → elevated cutting temperature → further degradation of thermal conductivity → accelerated tool wear. Liquid nitrogen cooling breaks this cycle by maintaining the cutting zone at temperatures where the material retains higher thermal conductivity (33.94 W/mK at room temperature vs 29.83 W/mK at 300°C), thereby enhancing heat dissipation efficiency.

3.5.2 Thermal-wear coupling effects

The 22.38% reduction in average cutting temperature under liquid nitrogen cooling (201.9°C vs 260.1°C) directly impacts tool wear progression. The lower temperature environment preserves the hard coating integrity of the cutting tool, as demonstrated by the distinct performance divergence beyond 3000m cutting length. Below this threshold, both cooling methods show comparable performance because the coating remains functional. However, once the coating wears through under cutting fluid cooling, the rapid deterioration begins.

The real-time temperature curves provide further insight into this mechanism. The stable temperature profile under liquid nitrogen cooling indicates consistent tool-workpiece contact, while the fluctuating temperatures with cutting fluid suggest unstable contact conditions due to alternating adhesion and fracture at the tool-chip interface. This instability accelerates wear and contributes to the rapid increase in surface roughness beyond 3000m cutting length.

4 Conclusions

This study reveals a coupled mechanism of cryogenic embrittlement of CGI-400 and preservation of tool coating integrity under liquid nitrogen cooling, advancing the understanding of CGI cryogenic machining from a purely thermal view to a thermal–mechanical–adhesive coupling view. The main conclusions are as follows:

- (1) Liquid nitrogen cooling improves machinability through a dual mechanism: it induces cryogenic embrittlement of CGI-400, reducing tensile strength by 11.32% (373.8 to 331.5 MPa) and promoting brittle chip

formation, while simultaneously decreasing the average cutting temperature by 22.38% (260.1 to 201.9 °C), thereby maintaining tool coating integrity. This interrupts the detrimental cycle caused by the 12.1% decrease in thermal conductivity of CGI-400 from 23 to 300 °C (33.94 to 29.83 W/mK).

- (2) Beyond a critical cutting length of 3000 m, the advantages of liquid nitrogen cooling become significant: surface roughness remains stable at 2.1–2.2 μm (vs. 2.3–2.4 μm under cutting fluid cooling), and flank wear is reduced by approximately 30%, demonstrating its effectiveness in extending tool life during prolonged machining.
- (3) EDS analysis reveals that liquid nitrogen cooling alters the wear mechanism: cutting fluid cooling causes complete Fe coverage and severe built-up edge formation, whereas liquid nitrogen cooling results in only local adhesion with no built-up edge, shifting the wear mechanism from adhesive to milder abrasive wear and preserving the protective coating.
- (4) The main limitations are that cryogenic embrittlement was evaluated by immersion rather than in-situ thermal cycling, temperature was measured at a single point, and only one set of cutting parameters and one insert type were tested. Future work should establish a predictive model linking cryogenic parameters, coating integrity, and tool life for industrial application.

Acknowledgement

This research was funded by Zhejiang Provincial Natural Science Foundation of China under Grant (LQN25E050017), the Fundamental Research Funds for the Provincial Universities of Zhejiang (GK259909299001-035), the Young Scientists Fund of the National Natural Science Foundation of China (52305530, 12202128), and the Ninth China Association for Science and Technology Youth Talent Lift Project Support Plan (YESS20230359).

References

[1] ZHENG L. J., LAI Z. W., SUN Y., et al. The machining of compacted graphite irons - State of the art and future perspective[J]. *Machining Science and Technology*, 2025, 29(1): 118-157.

[2] TAN J., WANG J. P., HAO X. Q., et al. Research on coated wiper insert for milling of compacted graphite iron[J]. *The International Journal of Advanced Manufacturing Technology*, 2024, 132(3-4): 1237-1249.

[3] JAN B.. Measurement of heat transfer in a sand mould foundry – optimisation of cooling time for cast iron and ductile cast iron mass castings[J]. *Manufacturing Technology*, 2025, 25(2): 161-169.

[4] WOLLMANN D., DE MIRANDA M. A., PINTAUDE G., et al. Abrasive wear resistance of high-strength compacted graphite iron under microabrasion conditions[J]. *Lubricants*, 2022, 10(11): 308.

[5] GRZESIK W., RECH J., ŻAK K., et al. Machining performance of pearlitic ‑ ferritic nodular cast iron with coated carbide and silicon nitride ceramic tools[J]. *International Journal of Machine Tools and Manufacture*, 2009, 49(2): 125-133.

[6] MALAKIZADI A., SADIK I., NYBORG L. Wear mechanism of CBN inserts during machining of bimetal aluminum-grey cast iron engine block[J]. *Procedia CIRP*, 2013, 8: 188-193.

[7] TOOPTONG S., PARK K. H., KWON P. A comparative investigation on flank wear when turning three cast irons[J]. *Tribology International*, 2018, 120: 127-139.

[8] ABELE E., SAHM A., SCHULZ H. Wear mechanism when machining compacted graphite iron[J]. *CIRP Annals-Manufacturing Technology*, 2002, 51(1): 53-56.

[9] LINDVALL R., DIAZ K. M., PENG R. L., et al. Wear mechanisms in Ti(C,N)-Al2O3 coated carbide during sustainable machining CGI[J]. *International Journal of Refractory Metals and Hard Materials*, 2024, 119: 106550.

[10] MOHAMMED W. M., NG E., ELBESTAWI M. A. Modeling the effect of the microstructure of compacted graphite iron on chip formation[J]. *International Journal of Machine Tools and Manufacture*, 2011, 51(10-11): 753-765.

[11] ONDREJ B., JAN O., PETR J., et al. Microtexturing for enhanced machining: evaluating tool performance in laser-processed cutting inserts[J]. *Manufacturing Technology*, 2024, 24(2):173-182.

[12] QIU Y., PANG J. C., LI S. X., et al. Influence of thermal exposure on microstructure evolution and tensile fracture behaviors of compacted graphite iron[J]. *Materials Science and Engineering: A*, 2016, 664: 75-85.

[13] AKINRIBIDE O. J., OGUNDARE O. D., OLUWAFEMI O. M., et al. A review on heat treatment of cast iron: phase evolution and mechanical characterization[J]. *Materials*, 2022, 15(20): 7109.

[14] SUHAIMI M. A., PARK K. H., YANG G. D., et al. Effect of cryogenic high-speed milling of compacted graphite iron using indirect spray system[J]. *International Journal of Advanced Manufacturing Technology*, 2018, 99: 2149-2157.

[15] NGUYEN D., TOOPTONG S., PARK K. H., et al. Formation mechanism of alumina layer in protecting cubic boron nitride inserts in turning cast irons[J]. *International Journal of Machine Tools and Manufacture*, 2020, 153: 103539.

[16] RAO S. V., RAMANA M. V., KUMAR A. C. S. An experimental investigation on Compact Graphite Iron wear behavior at 32℃ and 200℃[J]. *Materials Today: Proceedings*, 2019, 19: 778-780.

[17] ARAMCHAROEN A., CHUAN S. K. An experimental investigation on cryogenic milling of Inconel 718 and its sustainability assessment[J]. *Procedia CIRP*, 2014, 14: 529-534.

[18] WANG C. Y., LIN H. S., WANG X., et al. Effect of different oil-on-water cooling conditions on tool wear in turning of compacted graphite cast iron[J]. *Journal of Cleaner Production*, 2017, 148: 477-489.

[19] SUHAIMI M. A., PARK K. H., YANG G. D., et al. Effect of cryogenic high-speed milling of compacted graphite iron using indirect spray system[J]. *International Journal of Advanced Manufacturing Technology*, 2018, 99: 2149-2157.

[20] MENG F. N., ZHANG Z. Y., LI J. Q., et al. A novel approach of composite turning for compacted graphite iron using minimum quantity lubrication and liquid nitrogen jetting by a developed setup[J]. *Journal of Manufacturing Processes*, 2024, 117: 278-288.

[21] TU L. Q., CHEN J., AN Q. L., et al. Machinability improvement of compacted graphite irons in milling process with supercritical CO_2-based MQL[J]. *Journal of Manufacturing Processes*, 2021, 68: 154-168.

[22] LIN H. S., WANG C. Y., LUO J., et al. Performance of tool with hard coating when cutting compacted cast iron under different spray filed[J]. *Diamond and Abrasives Engineering*, 2019, 39(3): 51-57.

[23] KUZU A. T., BIJANZAD A., BAKKAL M. Experimental investigations of machinability in the turning of compacted graphite iron using minimum quantity lubrication[J]. *Machining Science and Technology*, 2015, 19: 559-576.

[24] TOOPTONG S., PARK K. H., LEE S. W., et al. A preliminary machinability study of flake and compacted graphite irons with multilayer coated and uncoated carbide inserts[J]. *Procedia Manufacturing*, 2016, 5: 644-657.

[25] NING K., WANG Q., WANG J., et al. Wear-resistant and anti-corrosion mechanism for transmission friction pairs in marine environment[J]. *Friction*, 2025, 13(9): 9441037.

[26] MENG F. N., ZHANG Z. Y., WU B., et al. Turning processes and mechanism of compacted graphite iron used for high performance engine[J]. *Journal of Manufacturing Processes*, 2021, 68: 951-960.

[27] Krzysztof K., Pavol G.. Analysis of the impact of modernization of machinery on the quality of castings using quality management tools[J]. *Manufacturing Technology*, 2024, 24(2):207-218.

[28] LONG F., SONG K. X., ZHANG Z. Q., et al. Research progress on brazing copper with dissimilar materials[J]. *Rare Metal Materials and Engineering*, 2025, 54(3): 818-836.